

Influence of Precracking Procedure, Environment, Temperature and Microstructure on *R*-Curve Behaviour of Alumina and PSZ Ceramics

M. Saadaoui,* C. Olagnon & G. Fantozzi

G.E.M.P.P.M. URA No. 341, I.N.S.A. Bât. 502, 69621 Villeurbanne Cedex, France

(Received 18 January 1993; revised version received 3 June 1993; accepted 24 June 1993)

Abstract

R-Curve behaviour of alumina and magnesia partially stabilized zirconia (PSZ) has been investigated. The influence of precracking procedure (notch or pop-in precrack), the environment, the temperature and microstructure has been studied. Alumina and high monoclinic phase content PSZ show similar behaviour, different from that observed for high tetragonal phase content PSZ. The results are discussed in terms of microstructure, fracture mode and toughening mechanisms.

Das *R*-Kurvenverhalten von Aluminiumoxid und mit Magnesiumoxid teilstabilisiertem Zirkoniumoxid wurde untersucht. Der Einfluß der Rißeinleitungsmethode (Kerbe oder Härteindruck), der Umgebung, der Temperatur und des Gefüges wurden untersucht. Aluminiumoxid und PSZ mit einem hohen Anteil monokliner Phase zeigen ähnliches Verhalten, das sich vom Verhalten des PSZ mit hohem Anteil an tetragonaler Phase unterscheidet. Die Ergebnisse werden bezüglich des Gefüges, der Bruchart und des Zähigkeitszunahmemechanismuses diskutiert.

Les courbes de résistance à la propagation de fissures (courbes *R*) ont été déterminées pour une alumine et une zircone partiellement stabilisée à la magnésie. L'influence sur la courbe *R* de la procédure de préfissuration (entaille ou fissure naturelle), de l'environnement, de la température et de la microstructure a été étudiée. L'alumine et la zircone contenant un taux élevé en phase monoclinique ont des comportements identiques qui diffèrent de celui observé pour une zircone riche en phase tetragonale. Les résultats sont discutés en fonction de la microstructure, du mode de rupture et des mécanismes de renforcement mis en jeu.

* Present address: E.M.I., B.P. 765, Rabat, Morocco.

1 Introduction

Several studies conducted on polycrystalline alumina^{1–5} and partially stabilized zirconia (PSZ)^{6–10} have reported an increasing resistance to crack growth with crack extension (so called *R*-curve behaviour). Rising *R*-curve behaviour has been explained in terms of energy dissipation mechanisms such as microcracking,¹¹ wake-shielding by interlocking grain bridging,^{3,12–14} crack deflection or stress-induced phase transformation in zirconia-based ceramics.^{15,16}

The *R*-curve (crack growth resistance versus crack extension) which provides a more refined analysis compared to a single fracture parameter such as toughness, is now widely used to describe fracture of ceramic materials. Recent studies have attempted to take into account the influence of *R*-curve behaviour on other crack growth-related damage mechanisms. Particularly, Lutz & Swain^{17,18} have correlated flaw resistance and thermal shock behaviour of ceramics to their *R*-curve. They have shown that the slope of the *R*-curve is an indicator of the flaw resistance and the thermal shock degradation. Okada & Hirosaki¹⁹ have analysed the subcritical crack growth of sintered silicon nitride in terms of the *R*-curve behaviour and they have shown that a rising *R*-curve shifts the $v-K_I$ curve (subcritical crack growth rate versus applied stress intensity factor) to the high toughness region as the crack advances. Fett & Munz^{20,21} have shown from single-edge notched beam (SENB) tests under constant load that a rising *R*-curve behaviour can hinder subcritical crack growth. For alumina and PSZ materials, the $v-K_I$ curves obtained from the extension of saw cuts, exhibit a decreasing branch for low K_I values, i.e. subcritical crack growth rate decreases with increasing applied stress intensity factor.

Although it is of great importance for understanding the fracture behaviour of ceramics, there is

not, however, a unique R -curve for a material. It is strongly dependent on both testing and evaluation methods. In the case of alumina, several studies^{2,22} have shown that the R -curve depends on both microstructure and loading rate. Moreover, results have been shown to depend strongly on the testing method (i.e. SENB, DCB or DT tests), which have been explained by the interaction between crack opening displacement and microstructure, that varies with the sample geometry.

Renotching experiments after the extension of long cracks^{1,23,24} demonstrated that R -curve behaviour of alumina is 'wake' controlled: crack surface interaction by interlocking grain bridging in the wake is assumed to shield the crack tip from applied stresses.¹⁴ Additional energy dissipation in the wake region thus increases the fracture resistance as the crack advances.

For Mg-PSZ materials, it has been shown from SENB and DCB tests^{3,7,8,10} that the initiation energy and the R -curve amplitude depend on material microstructure. A high tetragonal phase content material shows a starting K_R value close to $7 \text{ MPa}\sqrt{\text{m}}$, which can reach $18 \text{ MPa}\sqrt{\text{m}}$ for a crack length increment of $500 \mu\text{m}$.⁸ However, it has also been shown²⁵ that an approach in terms of propagation energy, R , that takes into account the residual deformation after unloading, leads to a decreasing R -curve, which has been explained by transformation-induced plasticity at the crack tip.

The toughening mechanism is mainly due to tetragonal to monoclinic transformation for high tetragonal phase content, while microcracking and crack coalescence occurs in high monoclinic phase content material. Bridging was also observed⁸ in a low toughness PSZ in which a significant degree of intergranular fracture occurs.

The target of this work is to give more insights into the evaluation and understanding of R -curve behaviour of polycrystalline alumina and Mg-PSZ materials. The influence of the starting crack type, environment, temperature and microstructure on the crack growth resistance has been investigated.

2 Procedure

The materials used in this study were a commercial coarse-grained alumina ($30 \mu\text{m}$) 99.7% pure and a partially stabilized zirconia containing 9 mol% MgO (i.e. Mg-PSZ). Mg-PSZ is constituted of a cubic matrix containing tetragonal (t) and monoclinic (m) phase precipitates whose volumic proportions were varied by heat treatment. For this study, two distinct grades of material were retained: PSZ1 (28 vol.% t and 7.5 vol.% m precipitates) obtained after ageing at 1000°C for 1 h and PSZ2 (3 vol.% t

and 55 vol.% m) obtained by ageing at 1300°C for 6 h.

Controlled crack growth experiments were carried out under the three-point bending procedure (span 35 mm), with a crosshead speed of $2 \mu\text{m}/\text{min}$, on different environments (air, ethanol and water) at ambient and low temperatures.

Two different bend specimens were used: (i) single-edge notched beam (SENB) where a pre-notch has been introduced using a $300 \mu\text{m}$ diamond saw, followed by a thin notch made with a $70 \mu\text{m}$ saw, and (ii) single-edge precracked beam (SEPB) on which a sharp pop-in precrack was developed by the bridge indentation method,^{26,27} from three Vickers indentation cracks (100 N) regularly made on the sample face. Such cracks will be called 'natural' to distinguish them from sawn notches.

Specimen dimensions were typically $4 \times 6 \times 40 \text{ mm}^3$ and the initial precrack depth to sample width ratio, a_0/W , was chosen to be 0.6. The precracked samples were annealed for 15 min at 900°C to remove stresses due to the precracking procedure.

To characterize subcritical crack growth during stable propagation, a v - K_I relationship (K_I being the stress intensity factor and v the crack growth rate) was determined on the basis of acoustic emission (AE) counts. A piezo transducer was mounted on the end of the SENB sample and a crack was stably propagated from the notch tip to approximately 0.5 mm of the crack extension, then the loading machine was stopped. The load was gradually reduced because of subcritical crack growth and the AE was recorded during relaxation. The total number of AE counts, N , and the count rate, \dot{N} , were used to calculate the value of crack extension, Δa , and the crack growth rate, v , as follows:

$$\Delta a = \frac{a_f - a_i}{N_f} N \quad (1)$$

$$v = \frac{a_f - a_i}{N_f} \dot{N} \quad (2)$$

where a_i and a_f are the initial and the final values of the crack length, N_f is the total AE counts at the end of crack extension.

3 Calculation of the Crack Resistance Parameter

Loading curves of the studied PSZ materials show a significant deviation from linearity and residual crack-opening displacement was observed on both alumina and PSZ when specimens were completely unloaded.²⁸ Acoustic emission recorded during a cyclic loading procedure has shown²⁸ that the residual crack-opening displacement could be

attributed to debris formation that prevent crack closure.

To take into account the non-linearity of the loading curves, the crack growth resistance, R , was calculated using the graphical method of Sakai and coworkers^{29,30} based on a dimensionless load-displacement relationship. The results obtained for alumina and PSZ1 are compared to the fracture energy calculated as K_R^2/E (K_R being stress intensity factor and E the Young's modulus) when linear elastic behaviour is assumed (Fig. 1). It is clear that there is no significant difference between the two curves for both the two materials. The authors have therefore chosen to characterize the crack growth resistance of the materials studied in terms of the stress intensity factor, K_R , calculated assuming a linear elastic behaviour, as follows:

$$K_R = \sigma Y \sqrt{a} \quad (3)$$

where σ is the applied stress, a the crack length calculated from the specimen's compliance, and Y is the geometric factor proposed by Srawley.³¹

4 Results

4.1 Alumina

The effect of the initial precracking procedure on the R -curve behaviour of alumina has been investigated. The R -curves obtained with SENB and SEPB samples are compared (Fig. 2). For the last case the authors considered a specimen as-pop-in precracked and after annealing at 900°C for 15 min.

The initial applied stress intensity factor, measured on SEPB tests, has the same value before and after annealing and is equal to 4.6 MPa√m, which is much higher than that resulting from SENB tests, which typically give a value of 2.6 MPa√m. The as-pop-in precracked specimen does not, however, show any significant further increase. After annealing, a rapid increase in K_R was observed followed by a plateau value and a little decrease when the crack length to sample width ratio, a/W , reached 0.75.

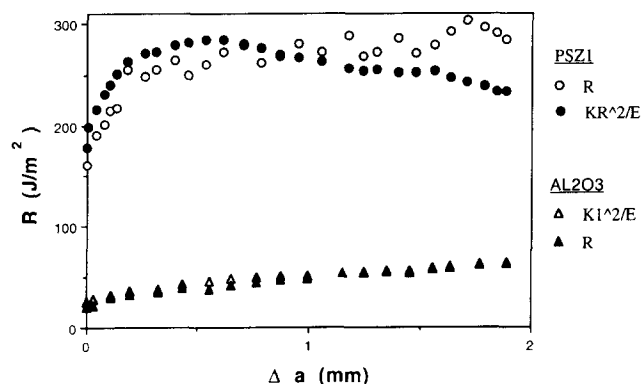


Fig. 1. R-Curves measured on SENB samples from dimensionless load-load point displacement curve and from K_R under the assumption of linear elastic behaviour.

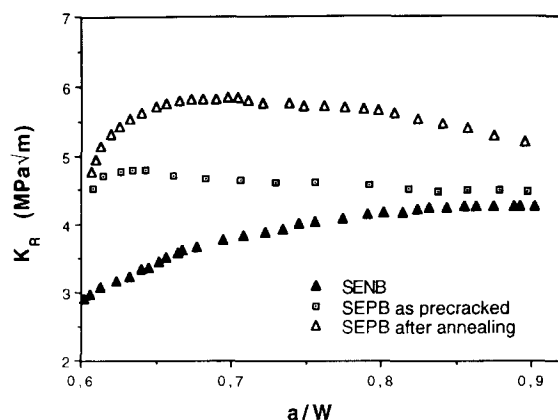


Fig. 2. Alumina. K_R -Curves from SENB and SEPB tests.

The difference observed between SEPB tests before and after annealing can be attributed to the relaxation by annealing of the residual stresses generally introduced during the pop-in-precracking procedure.³² The high level of K_R during the extension of long 'natural' cracks is a consequence of their stressed surfaces. Surface contact may lead to friction, interlocking or other dissipating mechanisms.

The influence of subcritical crack growth (SCG) on the K_R -curve has also been investigated by carrying out experiments under different environments as well as at low temperature. The K_R -curve has therefore been recorded in ethanol. In this case, the specimen was first held at 100°C for 3 h, then immersed for 30 min in ethanol before the experiment. The crack resistance curve obtained in ethanol is clearly above that obtained in air (Fig. 3). This result may be correlated with the subcritical crack growth reduction associated with a low moisture medium such as absolute ethanol. It is also important to note that the K_R reduction observed in air (with the SEPB test) after the maximum value is not present in ethanol.

The influence of slow crack growth has also been investigated with experiments conducted at -65°C (Fig. 4). The samples were cooled by projection of liquid nitrogen into a thermally insulated box and

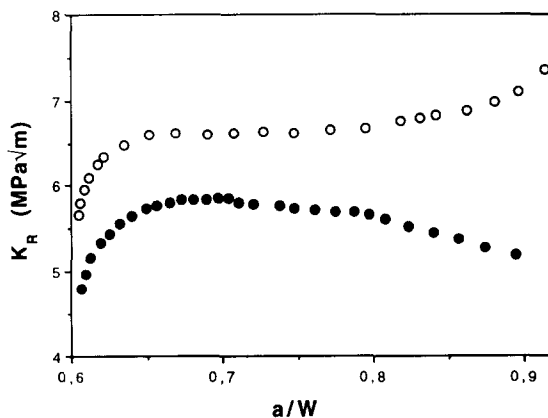


Fig. 3. Alumina. K_R -Curves measured (●) in air and (○) in ethanol (SEPB samples).

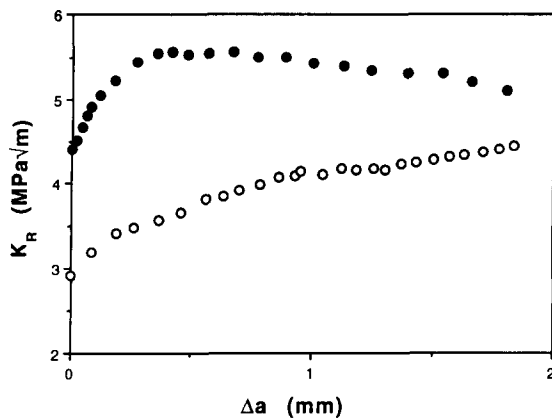


Fig. 4. Alumina. K_R -Curves (○) at ambient temperature (20°C) and (●) at -65°C (SENB samples).

the temperature was recorded with a thermocouple near the sample. The crack resistance curve at low temperature is clearly above that observed at 20°C. The high K_R value at the propagation onset may be attributed to subcritical crack growth decrease due to both the nitrogen atmosphere and the associated low temperature.

4.2 Zirconia

For comparison, the R -curves of the two Mg-PSZ grades have been recorded for SENB specimens (Fig. 5). For PSZ1 (higher tetragonal phase content), the initial value is about 5.6 MPa√m and rapidly rises to 7.8 MPa√m after 600 μm of crack extension, Δa , and decreases for further crack growth. Although the initial value observed for the PSZ2 sample is much lower, the rising domain is longer. The decrease of the K_R -curve after the rising part has been attributed to subcritical crack growth. Indeed, the maximum disappears when the tests are conducted at 10 μm/min displacement speed (Fig. 6) and a plateau region is observed.

The influence of the initial precrack on PSZ1 and PSZ2 is shown in Fig. 5. The K_R -curves of PSZ1 are very similar and therefore do not seem to depend on the starting crack. PSZ2 (high monoclinic phase

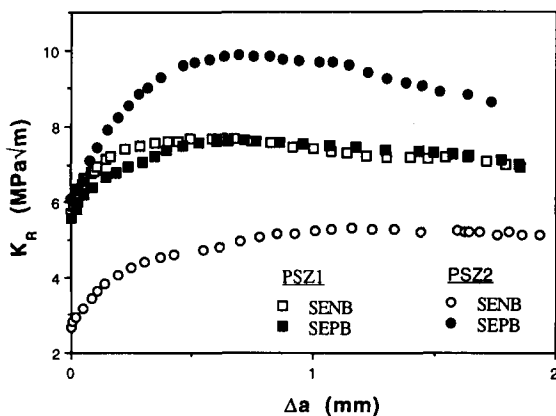


Fig. 5. K_R -Curves from SENB and SEPB samples of PSZ1 (high tetragonal phase content) and PSZ2 (high monoclinic phase content) materials.

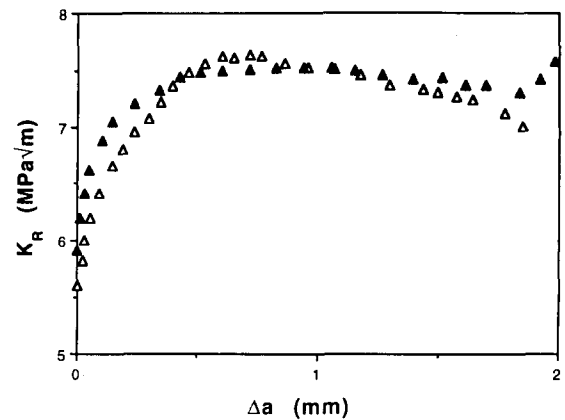


Fig. 6. Influence of displacement speed on the K_R -curve of PSZ1 material (SENB tests). Δ, 2 μm/min; ▲, 10 μm/min.

content) shows a different behaviour. The curve corresponding to the SEPB specimen is clearly above that determined with the SENB test. The initial and plateau values rise respectively from 2.8 and 5.3 to 6 and 9.8 MPa√m when starting with a 'natural' crack. This behaviour is similar to that observed for alumina.

The effect of subcritical crack growth has been investigated from experiments conducted in air, in water and in a low humidity medium. For PSZ1, while the starting parts of several environment K_R -curves coincide, the difference increases with crack extension (Fig. 7). The K_R decrease observed in air is significantly accentuated in water. Moreover, some instabilities have been observed in this latter case. In contrast, experiments conducted in alcohol lead to a continuously rising K_R -curve. The influence of the environment is very different in the case of the PSZ2 material. The different K_R -curves are systematically shifted to higher values with decreasing humidity (Fig. 7). Such a difference in behaviour also appears on the crack propagation rate versus crack extension curves (Fig. 8). For PSZ2 (Fig. 8(b)), the crack propagation rate seems to be independent of the environment. It increases regularly and goes through a maximum (the same behaviour has been observed on alumina). For the PSZ1 material (Fig. 8(a)), the crack growth rate is initially the same in

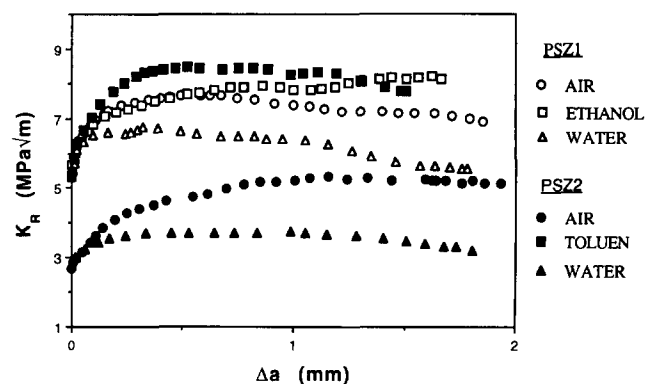


Fig. 7. K_R -Curves from SENB samples of PSZ1 and PSZ2 in different environments.

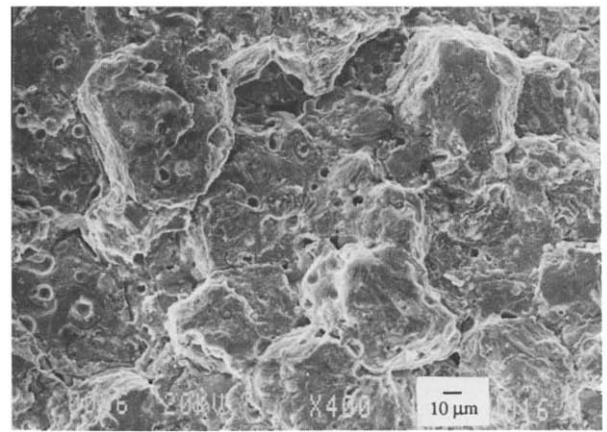
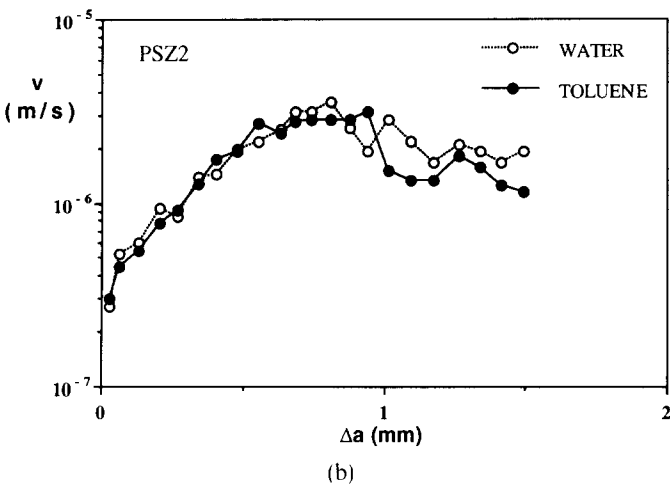
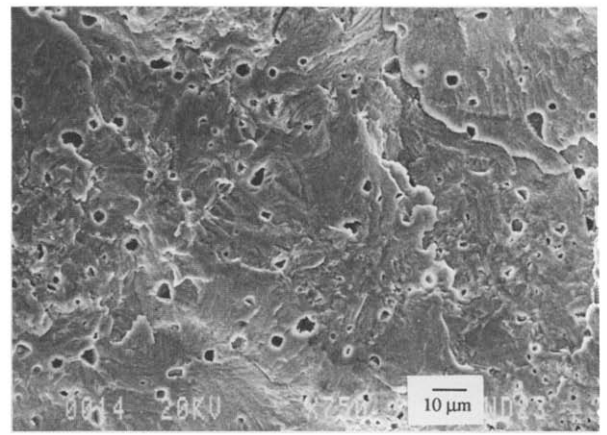
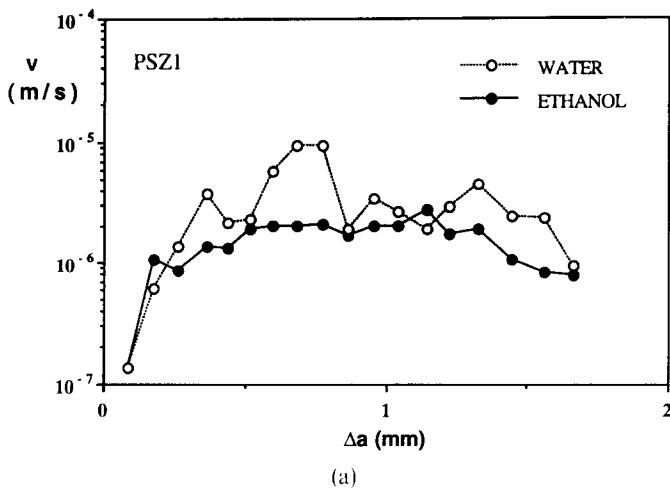


Fig. 8. Crack growth rate versus crack extension for (a) PSZ1 and (b) PDZ2 in different environments (SENB tests).

Fig. 10. SEM micrographs of fracture surface of (a) PSZ1 and (b) PSZ2 materials.

water and in ethanol. It increases regularly in ethanol, becomes nearly constant for Δa values in the range 0.5 mm to 1.4 mm and decreases for further crack growth, while it shows saw teeth variation in water, with high accelerations corresponding to crack instabilities observed on the loading curves.

K_R values obtained for PSZ1 at low temperature (-70°C) are again higher than those obtained at ambient temperature (Fig. 9). Observation of fracture surfaces (Fig. 10) show that the fracture of the PSZ1 material is mainly transgranular, while

that of the PSZ2 material is both trans- and intergranular.

5 Discussion

5.1 Precracking procedure

The comparison of the K_R -curves obtained for SENB and SEPB samples of alumina is in agreement with the crack-interface grain bridging mechanism that is generally used to explain R -curve behaviour of coarse-grained alumina.^{24,26,33} The applied stress intensity factor K_R can be written as follows:

$$K_R = K_{tip} + \Delta K_b \quad (4)$$

where K_{tip} is the stress intensity factor at the crack tip and ΔK_b the increase of the applied stress intensity factor due to grain bridging.

Bridging occurs within an interaction zone in the crack wake, resulting in compressive stresses along the crack surfaces which shield the crack tip from the applied stress. The extension of such a wake zone with crack propagation diminishes the driving force at the crack tip and thus increases the crack growth resistance.¹⁴ A saturation behaviour (plateau of the

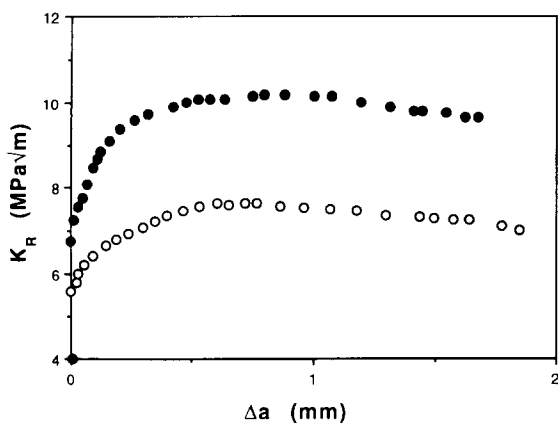


Fig. 9. K_R -Curves from SENB samples of PSZ1 (○) at ambient temperature (20°C) and (●) at -70°C .

R-curve) occurs when the crack opening displacement (COD) reaches a maximum value, δ_m , beyond which no further bridging occurs. The interaction zone also reaches a maximum length, z_m , and follows the crack tip.

It should be noted that when the controlled rupture experiment is conducted on an 'as-pop-in' pre-cracked specimen (before any annealing), no toughening is observed, which means that the wake interaction zone has been fully developed during the precracking procedure. Annealing the sample may lead to residual stress relaxation, but residual stresses are not fully annealed. On the other hand, friction due to contact between the long crack surfaces (promoted by intergranular fracture) persists even after annealing experiments.

To characterize *R*-curve behaviour of alumina, the extension of the interaction zone length, Δz , and the bridging stress, σ_b , were calculated from the plot of the stress intensity factor, K_R , as a function of the square root of the crack increment, $\sqrt{\Delta a}$.³⁴ This curve shows a linear part with a positive slope followed by a plateau region corresponding to the steady state regime.²⁸ The extension of the interaction zone length, Δz , corresponds to the crack extension at the beginning of the plateau region and σ_b is calculated from the slope of the curve using the expression:

$$K^* = K_0 + 4\sigma_b \sqrt{\frac{\Delta z}{2\pi}} \quad (5)$$

where K^* is the plateau value and K_0 the stress intensity factor at the onset of the stable crack propagation. K_0 therefore corresponds to the crack tip stress intensity factor, K_{tip} , for the SENB specimen, because no interaction initially exists between the crack surfaces. In the case of the SEPB specimen, K_0 is the sum of K_{tip} and some toughening contribution due to the pop-in precracking procedure. The crack opening displacement, δ_m , was also calculated from:³⁴

$$\delta_m = \frac{8}{E} \sqrt{\frac{\Delta z}{\pi}} \left[\sigma_b \sqrt{\frac{\Delta z}{\pi}} + \frac{K_0}{\sqrt{2}} \right] \quad (6)$$

The results are reported in Table 1 for SENB and SEPB samples. The bridging stress value is in good agreement with values reported in the literature for similar materials.^{12,23} The bridging stress value obtained for SEPB is larger owing to the residual

stresses exerted on crack surfaces. For SENB specimens, no interaction initially exists between the notched surfaces. The wake bridging zone begins to develop during the controlled crack propagation (*R*-curve test) and reaches its maximum length, z_m , at the onset of the *R*-curve plateau. Thus in this case $\Delta z = z_m$. For SEPB specimens, the development of the interaction zone begins during the pop-in precracking procedure, so the length Δz calculated from the K_R -curve corresponds only to the further extension of such a zone and not to its maximum length, as is the case for SENB specimens. This explains why a lower Δz value is obtained in this case.

It should be noted that the maximum COD has nearly the same value when measured on SENB or SEPB samples. However, it is less than the value of $7.5 \mu\text{m}$ predicted by Steinbrech *et al.*¹⁴ from the relation $\delta_m = D/4$, where D is the mean grain size. Grimes *et al.*²⁴ have also observed such a difference between the maximum COD measured from the *R*-curve and that predicted by the previous relation. This may be attributed to the non-homogeneity of grain distribution of the studied alumina. It contains coarse grains up to $100 \mu\text{m}$ and very small grains less than $10 \mu\text{m}$. The fracture mode is intergranular for small grains, while coarse grains fail in a transgranular mode and thus do not contribute to grain bridging. Grimes *et al.*²⁴ proposed to correlate the maximum COD to the largest grain which fails intergranularly, rather than to the average grain size.

According to their microstructure and toughening mechanisms, PSZ materials show different behaviours in the presence of long 'natural' cracks. Rising *R*-curve behaviour of PSZ1 is attributed to stress-induced phase transformation, while for PSZ2, in which tetragonal phase content is negligible, the predominant toughening mechanisms is interlocking grain bridging. The behaviour of the PSZ2 material is similar to that observed in alumina. The bridging parameters calculated from eqns (5) and (6) applied to a SENB specimen gives: $\sigma_b = 52.5 \text{ MPa}$, $z_m = 960 \mu\text{m}$ and $\delta_m = 3.7 \mu\text{m}$. This latter value is higher than that obtained for alumina according to the larger grain size of PSZ2 ($\approx 50 \mu\text{m}$) but it is again much less than the value of 12.5 that would be found from the relation proposed by Steinbrech *et al.*¹⁴

The use of SEPB samples rather than SENB ones leads to an inversion of the level of the K_R -curves of the two PSZ grades (Fig. 5). This can be explained by the increase of the wake contribution in SEPB samples of PSZ2, enhanced by intergranular fracture. The PSZ1 material fractured mainly in a transgranular mode, so crack surfaces interaction are negligible in this case. Annealing an SEPB

Table 1. Alumina bridging parameters determined for SENB and SEPB samples

	σ_b (MPa)	Δz (μm)	δ_m (μm)
SENB	32	676	1.05
SEPB	41	225	1.08

sample after the pop-in precracking procedure removes the stresses due to the phase transformation around the crack tip and in the wake. The crack surfaces become stress free and the behaviour is similar to that obtained with an SENB sample.

5.2 Subcritical crack growth

The stress intensity factor acting at the crack tip, K_{tip} , is generally considered as the result of two contributions, i.e.:

$$K_{tip} = K_a - \Delta K_s \tag{7}$$

where K_a is the stress intensity factor caused by the applied stress and ΔK_s is the contribution of shielding mechanisms, depending on microstructure.

In the absence of any subcritical crack growth, equilibrium is obtained when the stress intensity factor at the crack tip just balances the intrinsic toughness, K_0 , associated with the creation of crack surfaces:

$$K_{tip} = K_0 \tag{8}$$

According to this, eqn (7) can be restated as:

$$K_a = K_0 + \Delta K_s = K_R \tag{9}$$

Where K_R characterizes crack growth resistance force if no stress corrosion cracking occurs.

Under conditions of stress corrosion, SCG takes place, i.e. the crack propagates at a lower level of K_{tip} :

$$K_{tip} < K_0 \tag{10}$$

Thus, the stress intensity factor, K_a , calculated from the applied stress, is less than the value of K_R , which would be found under the same conditions in the absence of SCG:

$$K_a = K_{tip} + \Delta K_s < K_R \tag{11}$$

Increasing SCG decreases K_{tip} and thus diminishes the stress intensity factor experimentally measured from the applied load.

Crack growth resistance of alumina and partially stabilized zirconia is clearly influenced by environmentally assisted stress corrosion cracking. The SCG effect is, however, not the same for all materials studied, but seems to depend on microstructure and toughening mechanisms. For PSZ1, stress-induced transformation delays the SCG effect: the reduction of K_{tip} due to moisture stress corrosion is counteracted by the increase of the shielding contribution associated with transformation toughening at the onset of crack growth (rising part of K_R -curve). When the phase transformation contribution reaches its maximum (plateau region), it can not match the K_{tip} decrease, which leads to decreasing K_R -curves in air or in water, where stress corrosion is important. For alumina and PSZ2, the SCG

influence is observed at the onset of crack propagation, since the whole curve is shifted towards higher values of K_R in a low humidity environment. Interlocking grain bridging occurring in both materials does not allow the SCG effect to be delayed, which is promoted by intergranular fracture and by potential microcracking.

The high toughness value observed at low temperatures for alumina (Fig. 4) and PSZ1 (Fig. 9) is attributed to reduced subcritical crack growth. In the case of PSZ1, however, all the measured K_R -curves are shifted to a higher level at low temperature, while a reduction of humidity has no effect on the rising part of the curve. This can be explained by an increase in the thermodynamic driving force for tetragonal to monoclinic phase transformation, leading to a K_R increase at the early stage of propagation.

A plot of the v - K_I curves (crack growth rate versus stress intensity factor) obtained from the relaxation tests is shown in Fig. 11 for PSZ1 and PSZ2 materials. Unlike the results of Fett & Munz^{20,21} the curves have no decreasing branch, as the relaxation experiments have been carried out in the stationary toughening regime (i.e. plateau region of the K_R curve if no SCG occurs). The subcritical crack growth rate increases continuously with applied stress intensity factor and the slope of the data leads to n values for the usual power law fit to this curves ($v = AK^n$). n was found to be 130 to 140 for PSZ1 materials and 35 to 45 for PSZ2 materials. Although a limited range of crack velocities was investigated, those values are in a good agreement with results from double torsion samples, which give values of approximately 130 for PSZ1 and 45 for PSZ2³⁵ (Saadaoui, M. *et al.*, unpublished).

The results show that stress corrosion acts simultaneously with stable cracking in a humid

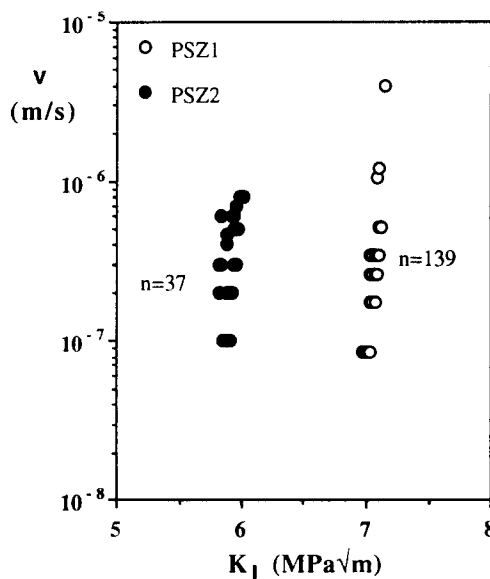


Fig. 11. v - K_I diagrams obtained from relaxation tests after stable cracking in three-point bending.

environment and diminishes the crack shielding effects due to the toughening mechanisms.

6 Conclusion

The use of a long crack on material exhibiting high intergranular fracture propensity dramatically increases the wake contribution, which determines the material toughness, and thus masks other toughening mechanisms. The *R*-curve differences determined by SEPB and SENB methods show that one can not extrapolate the toughness obtained from notched samples to the results that would be observed in the presence of long 'natural' cracks.

Environmentally assisted stress corrosion acts simultaneously with stable cracking in a humid environment. For the high tetragonal phase content PSZ, transformation toughening delays the subcritical crack growth effect in the rising part of the K_R -curve. In alumina and high monoclinic phase content PSZ, the SCG effect appears at the onset of the crack propagation, promoted by substantial microcracking.

References

- Knehans, R. & Steinbrech, R. W., Memory effect of crack resistance during slow crack growth in notched Al_2O_3 bend specimens. *J. Mater. Sci. Letters*, **1** (1982) 327–9.
- Deuerler, F., Knehans, R. & Steinbrech, R., Testing-method and crack resistance behaviour of Al_2O_3 . *J. Physique*, **47**(2) (1986) C1-618–C1-621.
- Swain, M. V., R-Curve behaviour in a polycrystalline alumina material. *J. Mater. Sci. Letters*, **5** (1986) 1313–15.
- Hubner, H. & Jillek, W., Sub-critical crack extension and crack resistance in polycrystalline alumina. *J. Mater. Sci.*, **12** (1977) 117–25.
- Steinbrech, R., Knehans, R. & Schaarwachter, W., Increase of crack resistance during slow crack growth in Al_2O_3 bend specimens. *J. Mater. Sci.*, **18** (1983) 265–70.
- Swain, M. V. & Hannink, R. H., R-Curve behaviour in zirconia ceramics. In *Advances in Ceramics, Science and Technology of Zirconia II*, Vol. 12, ed. N. Claussen, M. Ruhle & A. Heuer. American Ceramic Society, OH, 1984, pp. 225–39.
- Heuer, A. H., Transformation toughening in ZrO_2 -containing ceramics. *J. Am. Ceram. Soc.*, **70**(10) (1987) 689–98.
- Ready, M. J., Heuer, A. H. & Steinbrech, R. W., Crack propagation in Mg-PSZ. In *Advanced Structural Ceramics, Mater. Res. Soc. Symp. Proc.*, Vol. 78, ed. P. F. Becher, M. V. Swain & S. Somiya. Materials Research Society, Pittsburgh, PA, 1987, pp. 107–20.
- Marshall, D. B. & Swain, M. V., Crack resistance curves in magnesia-partially stabilized zirconia. *J. Am. Ceram. Soc.*, **71**(6) (1988) 399–407.
- Burns, S. J. & Swain, M. V., Fracture toughness of MgO-partially stabilized ZrO_2 specimens with K_R -curve behaviour from transformation toughening. *J. Am. Ceram. Soc.*, **69**(3) (1986) 226–30.
- Evans, A. G. & Faber, K. T., Crack growth resistance of microcracking brittle materials. *J. Am. Ceram. Soc.*, **67**(4) (1984) 255–60.
- Majumda, B. S., Rosenfield, A. R. & Duckworth, W. H., Analysis of *R*-curve behaviour of non-phase-transforming ceramics. *Eng. Frac. Mech.*, **31**(4) (1988) 683–701.
- Mai, Y. W. & Lawn, B. R., Crack interface grain bridging as a fracture resistance mechanics model. *J. Am. Ceram. Soc.*, **70**(4) (1987) 289–94.
- Steinbrech, R. W., Reichl, A. & Schaarwachter, W., R-Curve behaviour of long cracks in alumina. *J. Am. Ceram. Soc.*, **73**(7) (1990) 2009–15.
- McMeeking, R. M. & Evans, A. G., Mechanics of transformation toughening in ceramics. *J. Am. Ceram. Soc.*, **65**(5) (1982) 242–6.
- Marshall, D. B. & Evans, A. G., Transformation toughening in ceramics. In *Fracture Mechanics of Ceramics*, Vol. 6, ed. R. C. Bradt & A. G. Evans. Plenum Press, New York, 1983, pp. 299–307.
- Lutz, H. E. & Swain, M. V., Interrelation among flaw resistance, K^R -curve behaviour and thermal shock degradation in ceramics. I. Theoretical considerations. *J. Eur. Ceram. Soc.*, **8** (1991) 355–63.
- Lutz, H. E. & Swain, M. V., Interrelation among flaw resistance, K^R -curve behaviour and thermal shock degradation in ceramics. II. *J. Eur. Ceram. Soc.*, **8** (1991) 365–74.
- Okada, A. & Hirotsuki, N., Subcritical crack growth in sintered silicon nitride exhibiting a rising *R*-curve. *J. Am. Ceram. Soc.*, **73**(7) (1990) 2095–6.
- Fett, T. & Munz, D., Subcritical crack growth of macrocracks in alumina with *R*-curve behaviour. *J. Am. Ceram. Soc.*, **75**(4) (1992) 958–63.
- Fett, T. & Munz, D., Subcritical crack growth of macrocracks in zirconia. *J. Mater. Sci. Letters*, **10** (1991) 1103–6.
- Steinbrech, R. W., Deuerler, F., Reichl, A. L. & Schaarwachter, W., Correlation of crack opening displacement and crack resistance curve of alumina. In *Science of Ceram.*, Vol. 14, ed. D. Taylor *et al.* The Institute of Ceramics, Canterbury, UK, 1988, pp. 659–64.
- Reichl, A. & Steinbrech, R. W., Determination of crack bridging forces in alumina. *J. Am. Ceram. Soc.*, **71**(6) (1988) C.299–C.301.
- Grimes, R. E., Kelkar, G. P., Guazzone, L. & White, K. W., Elevated temperature *R*-curve behaviour of a polycrystalline alumina. *J. Am. Ceram. Soc.*, **73**(5) (1990) 1399–404.
- Rose, L. R. F. & Swain, M. V., Two *R*-curves for partially stabilized zirconia. *J. Am. Ceram. Soc.*, **69**(3) (1986) 203–7.
- Warren, R. & Johannesson, B., Creation of stable cracks in hard metals using bridge indentation. *Powder Metall.*, **27**(1) (1984) 25–9.
- Nose, T. & Fujii, T., Evaluation of toughness for ceramic materials by a single-edge-precracked-beam method. *J. Am. Ceram. Soc.*, **71**(5) (1988) 328–33.
- Saadaoui, M., Crack growth resistance of alumina and zirconia ceramics. PhD Thesis, Institut National des Sciences Appliquées de Lyon, 1991 (in French).
- Sakai, M. & Inagaki, M., Dimensionless load–displacement relation and its application to crack propagation problems. *J. Am. Ceram. Soc.*, **72**(3) (1989) 388–94.
- Sakai, M. & Bradt, R. C., Graphical methods for determining the non-linear fracture parameters of silica and graphite refractory composites. *4th Int. Fract. Mech. Ceramics*, Vol. 7, VPI, 19–21 June 1985. Plenum Press, 1986, pp. 491–503.
- Srawley, J. E., Wide range stress intensity factor expressions of ASTM E 399 standard fracture toughness specimens. *Int. J. Fract.*, **12**(3) (1976) 475–6.
- Nishida, T., Shiono, T. & Nishikawa, T., On the fracture toughness of polycrystalline alumina measured by SEPB method. *J. Eur. Ceram. Soc.*, **5** (1989) 379–83.
- Swanson, P. L., Fairbanks, C. J., Lawn, B. R., Mai, Y. W. & Hockey, B. J., Crack–interface grain bridging as a fracture resistance mechanism in ceramics: I. Experimental study of alumina. *J. Am. Ceram. Soc.*, **70**(4) (1987) 279–89.
- Sakai, M., Yoshimura, J. I., Goto, Y. & Inagaki, M., R-Curve behaviour of a polycrystalline graphite: microcracking and grain bridging in the wake region. *J. Am. Ceram. Soc.*, **71**(8) (1988) 609–16.